# SUPERSONIC TURBULENT FLOW IN AXISYMMETRIC NOZZLES AND DIFFUSERS

**Somnath Ghosh, Joern Sesterhenn and Rainer Friedrich**
Fachgebiet Strömungsmechanik,
Technische Universität München
Boltzmannstr. 15, D-85748 Garching, Germany
Somnath.Ghosh@aer.mw.tum.de

## ABSTRACT

Effects of extra strain and dilatation rates on the turbulence structure in nozzles and diffusers with fully developed supersonic pipe flow as inflow condition are investigated by means of DNS and LES using high-order numerical schemes. It is found that weak pressure gradients already strongly inhibit or enhance the Reynolds stresses via corresponding changes of production and pressure-strain terms. The results constitute a database for the improvement of turbulence models for compressible flow.

## INTRODUCTION

Compressibility effects in simple turbulent shear flows along isothermal walls, like fully developed channel or pipe flow, manifest themselves in terms of mean density and temperature gradients in the near-wall layer and thereby increase the anisotropy of the Reynolds stress tensor. While the peak value of the streamwise Reynolds stress grows with increasing Mach number, the peak values of the other stresses decrease as a consequence of reduced pressure-strain correlations. Since wave-propagation effects are unimportant up to supersonic Mach numbers, solutions of the Poisson equation for the pressure fluctuations by means of a Green function have proven for fully-developed supersonic channel flow (Foysi et al. 2004) that the decrease in mean density from the wall to the channel core explains the decrease of all pressure-strain correlations compared to incompressible flow. Analogous effects hold for pipe flow. Now, the production of the streamwise Reynolds stress declines with increasing Mach number, but scales with the wall shear stress and the local viscosity along the semi-local wall-normal coordinate. The corresponding pressure-strain correlation does not follow this scaling law, and decreases faster with increasing Mach number which explains the increase in streamwise Reynolds stress.

There is a lack of knowledge concerning the response of compressible wall-bounded turbulence to acceleration and deceleration in axisymmetric nozzles and diffusers. The response leads to phenomena which cannot be explained in terms of mean property variations alone. Density, e.g. is not a direct function of pressure, so that vorticity may be produced through baroclinic torques. Moreover, dilatation effects generate vorticity directly or contribute to the decay of vorticity. Bradshaw (1974, 1977) has used the appropriate term 'complex flows' to denote flows in which significant pressure gradients and strain rates exist. He has discussed the increase in Reynolds stresses by bulk compression and their decrease by bulk expansion in supersonic turbulent boundary layers and has highlighted the need to improve engineering calculation methods. His attempt to account for mean dilatation effects in his empirical Reynolds shear stress equation provides some, but not sufficient improvement in predicting complex compressible flows. In their review article on the physics of supersonic turbulent boundary layers Spina et al. (1994) note a lack of knowledge with respect to the influence of extra rates of strain and trace it back to the scarcity of systematic high-quality measurements.

It is the aim of this paper to contribute new findings about effects of extra strain and dilatation rates on the turbulence structure in supersonic nozzles and diffusers using well-established and accurate numerical methods. The flow configuration chosen is fully-developed supersonic pipe flow subjected to gradual acceleration/deceleration in a nozzle/diffuser with a cooled isothermal wall. While this is one of the simplest ways to subject a pipe flow to a pressure gradient in an experimental setup, the computation of this kind of flow requires proper specification of inflow and outflow conditions. Large-eddy simulations of these flows using an explicit filtering version of the approximate deconvolution method (ADM) of Stolz and Adams (1999) have been undertaken here. A DNS has also been performed to validate the LES data for nozzle flow.

## NUMERICAL DETAILS OF DIRECT AND LARGE-EDDY SIMULATIONS

The governing Navier-Stokes equations are solved in a special pressure-velocity-entropy form (Sesterhenn, 2001) on non-orthogonal curvilinear coordinates using 6th order compact central schemes (Lele, 1992) for spatial discretizations in the LES. In the DNS, 5th order compact upwind schemes (Adams et al., 1996) have been used for the convection terms and 6th order compact central schemes for the molecular transport terms. The flow field is advanced in time in both cases using a 3rd order low-storage Runge-Kutta scheme (Williamson, 1980). ADM, implemented as a single-step explicit filtering approach (Mathew et al., 2003), is applied to treat the interaction between resolved and unresolved scales. Ghosh et al. (2006) had performed DNS and LES of supersonic pipe flow with an isothermal wall using the above mentioned discretization and explicit filtering technique and found very good agreement between DNS and LES data concerning correlations that are dominated by large scales. In the present work, fully-developed supersonic turbulent air flow in a pipe serves as inflow condition for nozzle and diffuser flow. The walls are kept at constant temperature in both cases. The inlet Mach and friction Reynolds numbers for the nozzle are 1.5 and 245 and for the diffuser 1.8 and 280. While the Mach number $M$ is based on the speed of sound at wall temperature and the bulk velocity, the friction Reynolds number $Re_\tau$ is defined using the friction velocity $u_\tau = \sqrt{\tau_w/\rho_w}$, the pipe radius $R$

and the kinematic viscosity at the wall, $\nu_w(T_w)$. The domain length of each configuration (pipe or nozzle/diffuser) is $L = 10R$. The streamwise variation of the flow cross section is calculated using streamtube equations for a given streamwise pressure distribution. This is done to ensure that the turbulence is subjected to an extended region of nearly constant weak pressure gradient. The average pressure gradients, normalized with the momentum thickness and the wall shear stress are -1.2 and 1.65 for nozzle, resp. diffuser flow. The ratio of nozzle- and diffuser-radius to pipe radius at the end of the computational domains is 1.58 (nozzle) and 0.93 (diffuser). The number of grid points used to discretize these domains is $64 \times 64 \times 50$ in the LES and $256 \times 128 \times 91$ in the DNS in streamwise, circumferential and radial directions. Similar spatial resolutions were shown to be adequate for DNS/LES of turbulent pipe flow at $M = 1.5$ and $Re_\tau = 245$ (Ghosh et al., 2006). The periodic pipe and nozzle/diffuser flow simulations are coupled using MPI routines. The concept of characteristics is applied to set inviscid inflow conditions for the spatially developing flows. The incoming characteristics are computed from the periodic pipe flow simulations and are received at every time-step in the nozzle/diffuser computation through MPI. For the viscous terms at the inflow, the streamwise derivatives are computed on a mixed stencil involving points from the pipe and the nozzle/diffuser simulations. Partially non-reflecting outflow conditions (Poinsot,Lele, 1992) are used in the subsonic region of the outflow plane. The streamwise derivative of the shear stresses parallel to the outflow plane and that of the heat flux through the outflow plane are set to zero as conditions on viscous terms. No sponge layer has been used either in the LES or in the DNS.

## RESULTS

Results are presented in two sections. In the first we discuss mean flow features in the nozzle, the evolution of Reynolds stresses and Reynolds stress budgets with a focus on pressure-strain correlations and the various contributions to production. Most of the results are based on LES data. DNS data are occasionally used to validate the results. The second section concentrates on analogous effects in the diffuser. Here, only LES data are available.

### Nozzle flow

For an improved understanding of compressibility and acceleration effects it is necessary to discuss the behaviour of mean primitive flow variables first. Figure 1 contains axial profiles of mean centerline Mach number and pressure (normalized with its value at inflow). Figure 2 shows profiles of mean temperature and density along the nozzle centerline. In both figures results obtained from isentropic streamtube equations have been plotted for comparison. Surprisingly, the mean core flow behaves close to accelerated isentropic flow with decreasing pressure, density and temperature. Figure 3 presents the streamwise evolution of radial temperature and density profiles and a comparison of DNS and LES data, which proves good agreement. In fully developed pipe flow (x/L=0.0) mean density and temperature are directly linked in radial direction, since the radial pressure gradient is negligibly small. The heat generated by dissipation in the wall layer strongly increases the mean temperature and leads to a heat flux out of the pipe. The mean density in turn drops from its high wall value to a low core value and thus reduces the pressure-strain correlations. This effect, explained for turbulent channel flow by Foysi et al.(2004), also holds for pipe flow. The described direct coupling between temperature and density in radial direction persists in the present accelerated flow (Figure 3, $x/L > 0.0$). While in the nozzle core adiabatic cooling due to acceleration compensates dissipative heating, this effect is less pronounced in the near-wall region. Due to flow acceleration in the nozzle the mean sonic line moves closer to the wall, so that the layer in which subsonic flow persists gets thinner in downstream direction. The strong increase in wall shear stress due to acceleration and the weaker increase in mean density ratio combine in such a way that the Van Driest transformed velocity profiles develop as shown in Figure 4. Very similar effects were observed by Bae et al. (2006) in DNS of strongly heated air flow in pipes.

Flow acceleration dramatically affects the turbulence structure. The streamwise Reynolds stress, normalized with the local wall shear stress, decreases by nearly an order of magnitude, as seen in Figure 5. Due to non-equilibrium of the flow, $\tau_w$ is no longer a scaling parameter suitable for collapsing Reynolds stress profiles in the core region, as is the case for fully-developed pipe flow (Ghosh et al., 2006). Figure 5 also evaluates the LES data by comparison with DNS data. The slight overshoot of the peak value in the LES is a consequence of ADM which does not account for the local anisotropy of the velocity fluctuations. Figure 6 presents the downstream evolution of the Reynolds shear stress and the total stress. Here again, a dramatic decrease of all terms in flow direction is observed. What is not shown due to lack of space is a similar strong decay of the solenoidal TKE dissipation rate and a decrease of the peak value of the turbulent Mach number from 0.25 to 0.17.

In order to understand the reasons for these changes in the nozzle, we examine production terms and pressure-strain correlations in the Reynolds stress budgets of $\overline{\rho u_x'' u_x''}/2$, $\overline{\rho u_x'' u_r''}$, $\overline{\rho u_r'' u_r''}/2$ and express them in a cylindrical $(x, \phi, r)$-coordinate system which differs only weakly from the computational coordinate system. In such a system the radial budget contains production terms as well. We distinguish between 'kinetic' and enthalpic production and split the first into contributions due to shear, extra rate of strain and mean dilatation. The 'kinetic' production terms are:

$$P_{xx} = \underbrace{-\overline{\rho u_x'' u_r''}\frac{\partial \widetilde{u_x}}{\partial r}}_{shear} \underbrace{-\frac{1}{3}\overline{\rho u_x'' u_x''}\frac{\partial \widetilde{u_l}}{\partial x_l}}_{mean\ dilatation} \underbrace{-\overline{\rho u_x'' u_x''}\left(\frac{\partial \widetilde{u_x}}{\partial x} - \frac{1}{3}\frac{\partial \widetilde{u_l}}{\partial x_l}\right)}_{extra\ rate\ of\ strain}$$

$$P_{xr} = \underbrace{-\overline{\rho u_r'' u_r''}\frac{\partial \widetilde{u_x}}{\partial r}}_{shear1} \underbrace{-\overline{\rho u_x'' u_x''}\frac{\partial \widetilde{u_r}}{\partial x}}_{shear2} \underbrace{-\frac{2}{3}\overline{\rho u_x'' u_r''}\frac{\partial \widetilde{u_l}}{\partial x_l}}_{mean\ dilatation} \underbrace{-\overline{\rho u_x'' u_r''}\left(\frac{\partial \widetilde{u_x}}{\partial x} + \frac{\partial \widetilde{u_r}}{\partial r} - \frac{2}{3}\frac{\partial \widetilde{u_l}}{\partial x_l}\right)}_{extra\ rate\ of\ strain}$$

$$P_{rr} = \underbrace{-\overline{\rho u_x'' u_r''}\frac{\partial \widetilde{u_r}}{\partial x}}_{shear} \underbrace{-\overline{\rho u_r'' u_r''}\left(\frac{\partial \widetilde{u_r}}{\partial r} - \frac{1}{3}\frac{\partial \widetilde{u_l}}{\partial x_l}\right)}_{extra\ rate\ of\ strain} \underbrace{-\frac{1}{3}\overline{\rho u_r'' u_r''}\frac{\partial \widetilde{u_l}}{\partial x_l}}_{mean\ dilatation}$$

Figures 7 and 8 show the contributions to $P_{xx}$ and $P_{xr}$ in the nozzle at $x/L = 0.45$ and in fully-developed pipe flow, normalized with local values of $\tau_w^2/\bar{\mu}$. Among the two production by shear terms in $P_{xr}$, the first is dominant and the second is negligible in this specific nozzle. Clearly, compressibility in the form of mean dilatation counteracts the shear production of the $\overline{\rho u_x'' u_x''}$, $\overline{\rho u_x'' u_r''}$ components. Acceleration (extra rate of strain) does the same, at least in the streamwise component. The production rates by shear are themselves reduced by the stabilization of the two stresses $\overline{\rho u_x'' u_r''}$ and $\overline{\rho u_r'' u_r''}$ . In the $\overline{\rho u_x'' u_x''}$-budget enthalpic production appears on the RHS in the form $-\overline{u_x''}\frac{\partial \bar{p}}{\partial x}$ and has only a very small positive value (not shown). The pressure-strain correlations can be split into deviatoric and dilatational parts:

$$\begin{aligned}
\Pi_{xx} &= \overline{p'\left(\frac{\partial u_x''}{\partial x} - \frac{d'}{3}\right)} + \frac{1}{3}\overline{p'd'}, \\
\Pi_{xr} &= \overline{p'\left(\frac{\partial u_r''}{\partial x} + \frac{1}{r}\frac{\partial r u_x''}{\partial r}\right)}, \\
\Pi_{rr} &= \overline{\frac{1}{r}p'\left(\frac{\partial r u_r''}{\partial r} - \frac{d'}{3}\right)} + \frac{1}{3}\overline{p'd'}
\end{aligned}$$

$d'$ represents dilatational fluctuations. Profiles of $\Pi_{xx}$, $\Pi_{xr}$, normalized with local values of $\tau_w^2/\bar{\mu}$, are presented in Figures 9, 10 for stations $x/L = 0.0, 0.45, 0.8$. The dramatic reduction of the deviatoric parts in the nozzle is obvious. The contribution of the pressure-dilatation correlation is very small. Besides the weak production by shear, the $\Pi_{rr}$-term is the only source term in the radial stress budget. The streamwise decay of $\overline{\rho u_r'' u_r''}$ is therefore mainly due to the reduction of the pressure-strain correlation which can be traced back to the reduction of pressure and velocity-gradient fluctuations. It remains to be shown which role mean dilatation, extra strain rate and mean density variation play in damping pressure fluctuations.

### Diffuser flow

Supersonic turbulent diffuser flow is not just the opposite of nozzle flow. Its behaviour strongly depends on the rate of deceleration. We recall that the inlet Mach and friction Reynolds numbers are 1.8 and 280. The chosen higher incoming Mach and Reynolds numbers (they were 1.5 and 250 for nozzle flow) avoid noticeable transonic regions at the end of the diffuser. Moreover, the axial profiles of centerline Mach number and pressure do not follow predictions of the isentropic streamtube equations, cf. Figure 11. Wall and centerline pressure distributions grow much faster due to trains of compression and expansion waves reminding us of shock trains observed in experiments at stronger flow deceleration (Matsuo et al. 1999). Figure 12 reveals that the mean temperature grows in the diffuser in flow direction due to compression and increased dissipation rate. As a consequence the mean density ratio decays in flow direction. The Van Driest transformed mean axial velocity now reaches levels higher than in fully developed pipe flow, see Figure 13. The Reynolds stresses increase due to enhanced turbulence activity. As an example we show the streamwise Reynolds stress in Figure 14 and the total as well as Reynolds shear stress in Figure 15. Although the flow deceleration is fairly weak (the centerline Mach number decreases from 1.8 to 1.45) the Reynolds stresses increase by roughly a factor of 2. As typical for decelerated wall bounded flow, the maximal shear stress moves away from the wall. We also note (without showing it) a growth in the solenoidal dissipation rate and the turbulent Mach number. The enhanced turbulence activity is reflected in the production of Reynolds stresses by mean shear, extra rate of strain and mean dilatation. Figure 16 shows that, in contrast to nozzle flow, mean dilatation and extra rates of strain now act as sources producing streamwise Reynolds stress. The first production by shear term (Figure 17) in the shear stress equation increases in a similar fashion as it decreases in the supersonic nozzle. The second term of this kind is now non-zero, but counteracts the first. Mean dilatation has a weak source effect. Finally, the pressure-strain correlations grow in decelerated flow and provide higher contributions to the radial and circumferential Reynolds stress components. The peak of the axial pressure-strain correlation in Figure 18 grows by a factor of at least five in the domain considered. The pressure-dilatation correlation taken at $x/L = 0.2$ is still very small compared to $\Pi_{xx}$. The axial growth of the radial pressure-strain correlation explains the growth of the radial Reynolds stress in the diffuser (not shown due to lack of space).

## CONCLUSIONS

Supersonic turbulent pipe flow subjected to gradual acceleration/deceleration in a nozzle/diffuser has been investigated by means of DNS and LES in order to assess the effects of mean dilatation and extra rate of strain on the turbulence structure. Although the rates of acceleration/deceleration are small, the decrease/increase in Reynolds stress components is large. At the same time dilatational fluctuations are only weakly affected, so that explicit compressibility terms (like pressure-dilatation and compressible dissipation rate) remain small. Among the source/sink terms in the Reynolds stress transport equations the production by shear, by extra-rate of strain, by mean dilatation and the pressure-strain correlations are strongly affected. It remains to be shown in which way extra-rates of strain, mean dilatation and mean density variations affect pressure and velocity-gradient fluctuations and thus control the variation of pressure-strain correlations. This is the aim of future work.

## REFERENCES


Adams, N.A., and Shariff, K., 1996, "A high-resolution hybrid compact ENO scheme for shock-turbulence interaction problems". Journal of Computational Physics, Vol. 127, pp. 27-51.

Bae, J.H., Yoo, J.Y., Choi, H., and McEligot, D.M., 2006, "Effects of large density variation on strongly heated internal air flows". Physics of Fluids, Vol. 18, pp. 075102-1/25.

Bradshaw, P., 1974, "The effect of mean compression or dilatation on the turbulence structure of supersonic boundary layers". Journal of Fluid Mechanics, Vol. 63, pp. 449-464.

Bradshaw, P., 1977, "Compressible turbulent shear layers". Annual Review of Fluid Mechanics, Vol. 9, pp. 33-52.

Foysi, H., Sarkar, S., and Friedrich, R., 2004, "Compressibility effects and turbulence scalings in supersonic channel flow". Journal of Fluid Mechanics, Vol. 509, pp. 207-216.

Ghosh, S., Sesterhenn, J., and Friedrich, R., 2006, "DNS and LES of compressible turbulent pipe flow with isothermal wall". Proceedings, Direct and Large-Eddy Simulation VI, E. Lamballais et al., ed., Springer, Dordrecht, pp. 721-728.

Lele, S.K., 1992, "Compact finite difference schemes with spectral-like resolution". Journal of Computational Physics,

Vol. 103, pp. 16-42.

Mathew, J., Lechner, R., Foysi, H., Sesterhenn, J., and Friedrich, R., 2003, "An explicit filtering method for large-eddy simulation of compressible flows". Physics of Fluids, Vol. 15, pp. 2279-2289.

Matsuo, K., Miyazato, Y., and Kim, H.D., 1999, "Shock train and pseudo-shock phenomena in internal gas flows". Progress in Aerospace Sciences, Vol. 35, pp. 33-100.

Poinsot, T.J., and Lele, S.K., 1992, "Boundary conditions for direct simulations of compressible viscous flows". Journal of Computational Physics, Vol. 101, pp. 104-129.

Sesterhenn, J., 2001, "A characteristic-type formulation of the Navier-Stokes equations for high-order upwind schemes". Computers and Fluids, Vol. 30, pp. 37-67.

Spina, E.F., Smits, A.J., and Robinson, S.K., 1994, "The physics of supersonic turbulent boundary layers". Annual Review of Fluid Mechanics, Vol. 26, pp. 287-319.

Stolz, S., and Adams, N.A., 1999, "An approximate deconvolution procedure for large-eddy simulation". Physics of Fluids, Vol. 11, pp. 1699-1701.

Williamson, J.K., 1980, "Low-storage Runge-Kutta schemes". Journal of Computational Physics, Vol. 35, pp. 48-56.

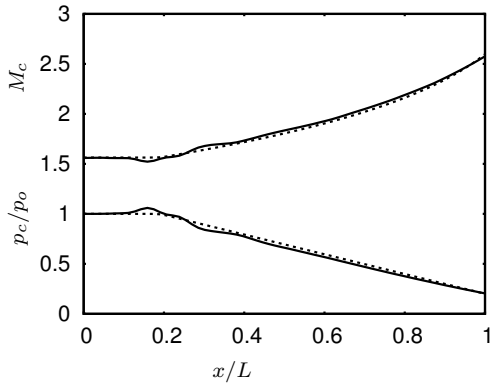


**Fig. 1:** Streamwise variation of mean centerline Mach number and pressure (normalized wth upstream value) in the nozzle. Dashed line: Isentropic streamtube result

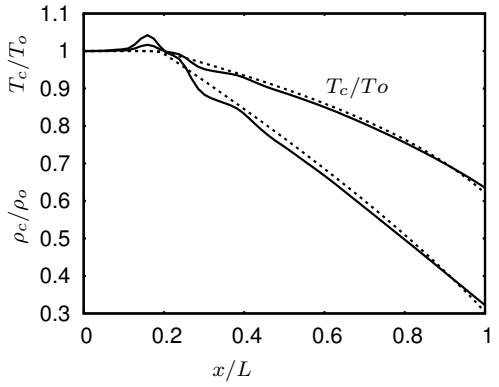


**Fig. 2:** Streamwise variation of mean centerline density and temperature (normalized wth upstream values) in the nozzle. Dashed line: Isentropic streamtube result

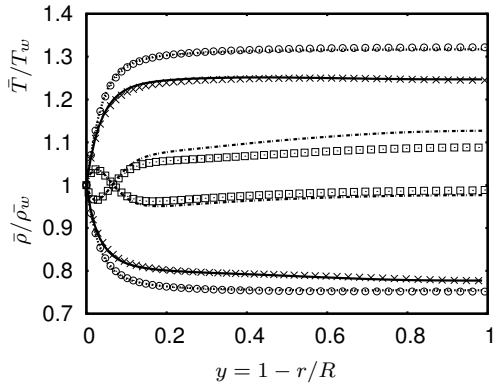


**Fig. 3:** Mean density and temperature profiles in the nozzle at stations $x/L = 0.0(\ldots\ \ldots), 0.45$ (—), $0.8(-.-.-)$. Lines: LES, symbols: DNS

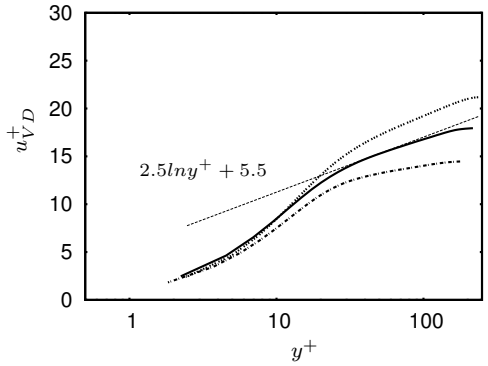


**Fig. 4:** Van Driest transformed mean velocity profiles in the nozzle. $x/L$ stations as in Figure 3

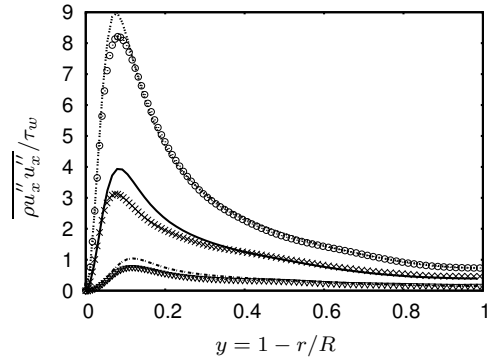


**Fig. 5:** Streamwise Reynolds stress in the nozzle normalized with local wall shear stress. $x/L$ stations as in fig. 3

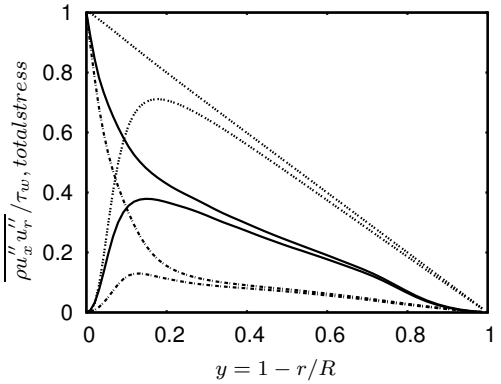


**Fig. 6:** Reynolds shear stress and total shear stress in the nozzle normalized with local wall shear stress. $x/L$ stations as in fig. 3

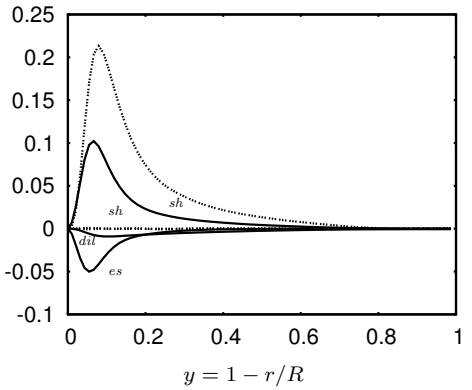


**Fig. 7:** Contributions to the production of the axial Reynolds stress in the nozzle at stations $x/L = 0.0$ (dashed line) and 0.45 (solid line) sh : mean shear, dil: mean dilatation, es: extra rate of strain

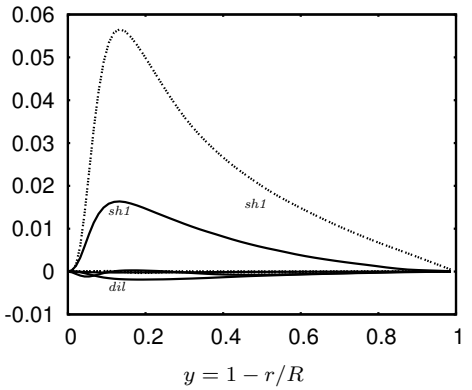


**Fig. 8:** Contributions to the production of the Reynolds shear stress in the nozzle at stations $x/L = 0.0, 0.45$. sh1: mean shear (*shear1*), dil: mean dilatation

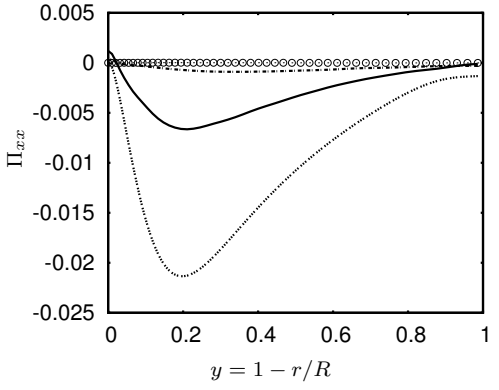


**Fig. 9** Pressure-strain correlation $\Pi_{xx}$ in the nozzle $x/L$ stations as in Figure 3. Symbols: $\overline{p'd'}/3$ at $x/L = 0.45$

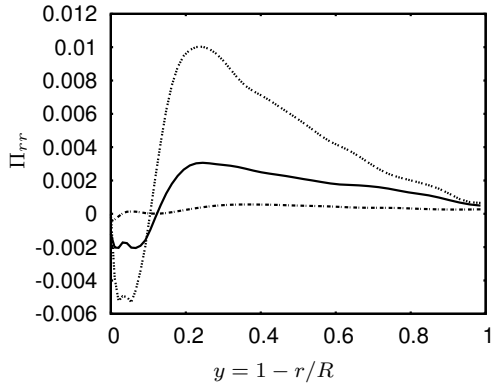


**Fig. 10** Pressure-strain correlation $\Pi_{rr}$ in the nozzle $x/L$ stations as in Figure 3.

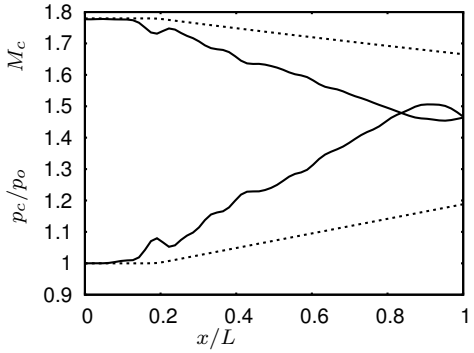


**Fig. 11:** Streamwise variation of mean centerline Mach number and pressure (normalized wth upstream value) in the diffuser. Dashed line: Isentropic streamtube result

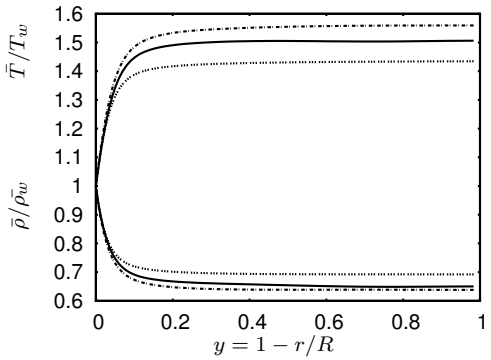


**Fig. 12:** Mean density and temperature profiles in the diffuser at stations $x/L = 0.0$(... ...), 0.2 (—), 0.45(−. − .−)

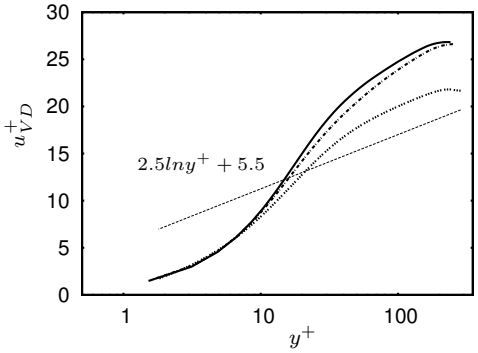


**Fig. 13:** Van Driest transformed mean velocity profiles in the diffuser. $x/L$ stations as in Figure 12

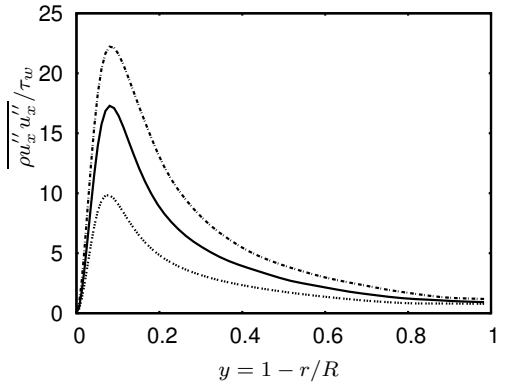


**Fig. 14:** Streamwise Reynolds stress in the diffuser normalized with local wall shear stress. $x/L$ stations as in fig. 12

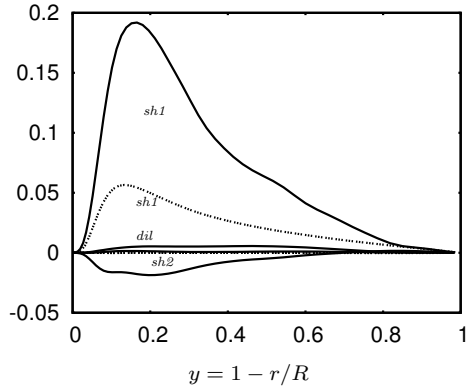


**Fig. 17:** Contributions to the production of the Reynolds shear stress in the diffuser at stations $x/L = 0.0, 0.2$. sh1: mean shear (*shear1*), sh2: mean shear (*shear2*), dil: mean dilatation

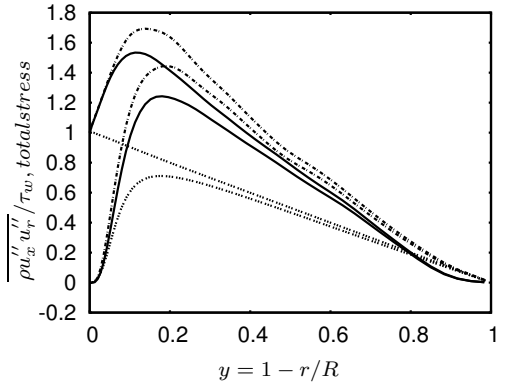


**Fig. 15:** Reynolds shear stress and total shear stress in the diffuser normalized with local wall shear stress. $x/L$ stations as in fig. 12

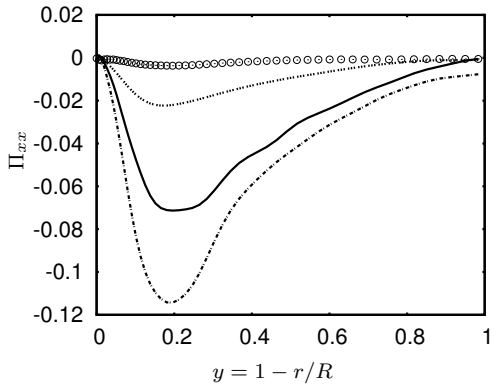


**Fig. 18** Pressure-strain correlation $\Pi_{xx}$ in the diffuser $x/L$ stations as in Figure 12. Symbols: $\overline{p'd'/3}$ at $x/L = 0.2$

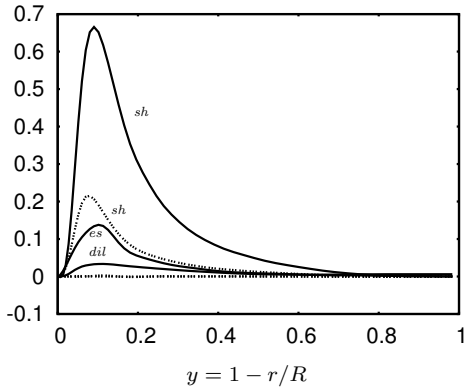


**Fig. 16:** Contributions to the production of the axial Reynolds stress in the diffuser at stations $x/L = 0.0$ (dashed line) and 0.2 (solid line) sh : mean shear, dil: mean dilatation, es: extra rate of strain

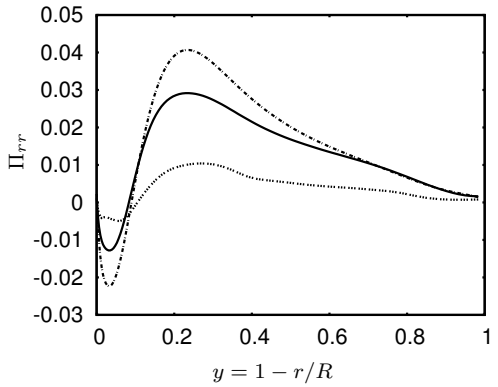


**Fig. 19** Pressure-strain correlation $\Pi_{rr}$ in the diffuser $x/L$ stations as in Figure 12